

UDC 535.81; 519.25

ENHANCING GAS DISTRIBUTION MAPPING RECONSTRUCTION ACCURACY THROUGH GEOMETRIC SCANNING TECHNIQUES

N.V. BACH

*Belarusian State University of Informatics and Radioelectronics, Republic of Belarus**Received March 28, 2025*

Abstract. Gas distribution mapping and source localization are critical for industrial safety, environmental monitoring, and hazard mitigation. This paper evaluates the influence of geometric scanning parameters on the reconstruction accuracy of gas distribution mapping using tunable diode laser absorption spectroscopy. The paper explores the interaction of laser light with gas molecules and surfaces, highlighting the role of absorption, scattering, and reflection in gas concentration measurement. Four laser scanning configurations are analyzed. Five tomographic algorithms are assessed for their effectiveness in reconstructing 2D gas distribution maps. The results demonstrate that the maximum-likelihood expectation maximization algorithm achieves the highest reconstruction accuracy across all configurations, while the triple fan-parallel beam scanning non-uniform distributed configuration offers the best overall accuracy.

Keywords: Gas distribution mapping, scanning configurations, laser light interaction, laser absorption.

Introduction

Gas distribution mapping (GDM) and source localization are critical tasks in various applications, including industrial plant inspections, landfill monitoring, and the detection of explosives or toxic gases at harbors and airports [1]. If the released gas is flammable and explosive, once it explodes, it will cause devastating damage to surrounding life and the environment, serious damage to the health of humans. Therefore, the normalized monitoring and prewarning of the source of hazardous gas leakage is of great importance.

Methods for GDM can be categorized into contact and noncontact measurements. Contact methods involve using semiconductors, electrochemical sensors, and similar technologies. These typically measure gas concentrations point by point using portable sensors or fixed sensor networks [2]. However, they often struggle to provide comprehensive spatiotemporal gas distribution data. Noncontact measurements include optical gas imaging (OGI) [3], laser absorption spectroscopy (LAS) combined with tomographic reconstruction techniques [4]. OGI utilizes infrared absorption properties to visualize gases, particularly effective in industrial settings for detecting gas leaks by providing real-time thermal images that highlight the location and extent of emissions. In contrast, LAS measures gas concentrations by analyzing laser beam absorption at specific wavelengths, using tomographic techniques to reconstruct gas distributions map. LAS generally offers higher accuracy in quantifying gas concentrations due to precise wavelength-dependent measurements, suitable for long-range detection and diverse environmental conditions. However, OGI provides immediate visual feedback for rapid identification and localization of gas leaks, although it may be limited by environmental factors affecting infrared imaging [5]. Laser spectroscopy techniques, such as tunable diode laser absorption spectroscopy (TDLAS), have garnered significant development in the field of trace gas detection in recent years due to their advantages of high sensitivity, precision [6].

Principle of TDLAS

The laser of the TDLAS sensor operates near the wavelength corresponding to the absorption spectrum of specific gas molecules, with absorption levels indicating the concentration of the target gas [7]. Transmitted laser intensity based on absorption, scattering and reflectance models is defined as

$$I_t(\lambda) = I_0(\lambda) \cdot K_r(\theta) \cdot (K_{abs}(y, l) \cdot K_{sca}(l))^2, \quad (1)$$

where $K_{sca}(l) = \exp(-K \cdot l)$ is the coefficient laser intensity attenuation according to the Rayleigh scattering [8, 9], the $K = 32\pi^3(\mu - 1)^2 / 3N_{mol}\lambda^4$ is the opacity coefficient, μ is the refractive index, are quantities experimentally measurable, λ is the wavelength of laser, N_{mol} is the number of molecules per unit volume, $K_{abs}(y, l) = \exp(-P \cdot y \cdot S(T) \cdot \phi(\lambda) \cdot l)$ is the coefficient laser intensity attenuation according to the Beer-Lambert law [7], y is the gas concentration along the laser path, l is the laser path length, P is the gas pressure, $\phi(\lambda)$ is the unity normalized line shape function, and $S(T)$ is the line strength function of temperature, I_0 is output laser intensity, $K_r(\theta)$ is the surface reflection coefficient, θ is the incidence angle of laser beam.

The average concentration of the optical path is determined by the relationship between the incident and transmitted light intensities based on optical reflectance, scattering and absorption models

$$y = \left(\ln \left(\frac{I_0(\lambda) \cdot K_r(\theta)}{I_t(\lambda)} \right) \cdot \frac{\cos \theta}{2 \cdot H} - K \right) \cdot \frac{1}{P \cdot S(T) \cdot \phi(\lambda)}, \quad (2)$$

where $H = l \cdot \cos \theta$ is the high of TDLAS sensor.

For reconstructing 2D image gas distribution mapping, tomographic reconstruction algorithm is used to solve ill-conditioned system of linear equations. Scanning the gas diffusion area to be measured using a TDLAS telemetry sensor (Figure 7), which collects concentration data y along the laser paths at multiple angles or intervals. Therefore, the whole region can be described by the vector Y and the mean gas concentrations in each cell can form a column vector X . Their relationship can be written as

$$\vec{Y} = \vec{L} \cdot \vec{X} + \varepsilon \vec{1}, \quad (3)$$

where $\vec{L} = (l_{ij})_{0 \leq i < M, 0 \leq j < N}$ the absorption path length value matrix that contains the absorption path length value $l_{i,j}$ of the i -th laser beam in the j -th cell matrix, $\vec{X} = (x_0, \dots, x_{N-1})^T$ and x_j are column vector concentration and the averaged gas concentration in cell j and $\vec{1}$ is a column vector of ones of length M , ε is the measurement noise term, M is the number of laser beam, N is the number of grid cell [6].

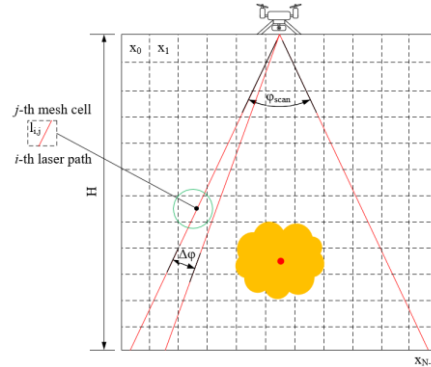


Figure 7. Laser scanning parameters and discretization configuration for gas diffusion area. The yellow area represents gas cloud

According to the measured matrix Y and the known absorption path length value matrix L , the concentration distribution X can be inversely calculated by tomographic algorithms.

Tomography algorithm

Least squares method (LSQR) is an iterative algorithm designed to solve large, sparse linear systems and least squares problems. Tikhonov regularization is widely used to stabilize solutions of ill-posed problems by introducing a regularization term that counteracts the amplification of noise [7]. Maximum-likelihood expectation maximization algorithm (MLEM) is an iterative method used to reconstruct the image by maximizing the likelihood function. It is particularly useful in scenarios with incomplete data. The method iteratively updates the solution to maximize the probability of the observed data given the model. Simultaneous algebraic reconstruction technique (SART) combines relaxation factors and iterative smoothing, providing better noise handling and convergence properties [6].

In order to evaluate the reconstruction quality of methane-diffusion distribution, the following three evaluation indexes are used to quantify the agreement between the original concentration field and the reconstructed result in this work. Three evaluation indexes: the normalized root mean square distance (NRMSD), the normalized average absolute distance (NAAD) and the gas-distribution map similarity coefficient (ϵ) [6].

Experimental result

The optical path configuration affects the reconstruction accuracy. In general, increasing the number of laser beams enhances reconstruction accuracy. However, to achieve an optimal balance between accuracy and computational efficiency, a thorough optimization and selection analysis are applied on the four laser scanning configurations illustrated in Figure 8.

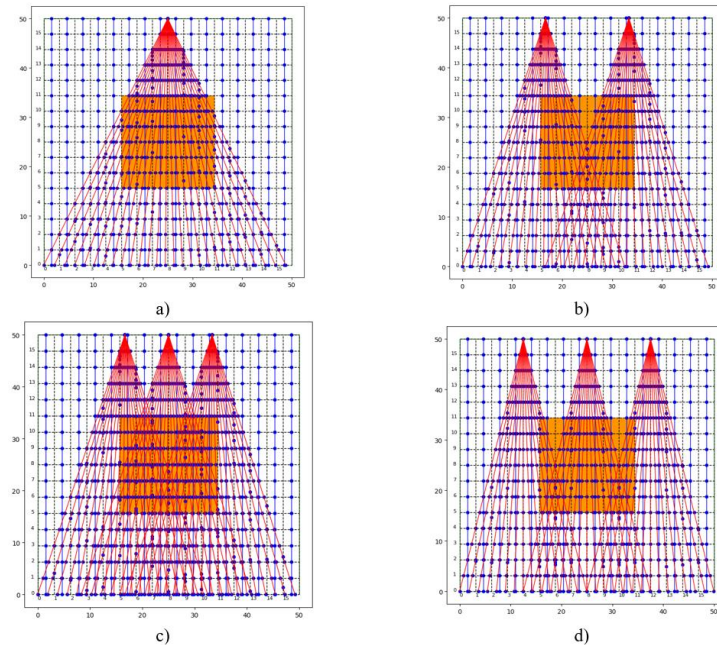


Figure 8. Laser-scanning coverage for the gas distribution mapping reconstruction based on a 16×16 grid discretized. Configurations of laser scanning: a) Single fan-parallel beam scanning (SFPS), b) Double fan-parallel beam scanning (DFPS), c) Triple fan-parallel beam scanning non-uniform distributed (TFPSN), d) Triple fan-parallel beam scanning uniform distributed (TFPSU). The green lines represent the parallel-beam optical paths. The red lines represent the fan-beam optical paths. The yellow area represents gas cloud.

Figure 9 shows the gas-distribution map similarity coefficient of different algorithms under 16×16 grid cells and different type of configurations of laser scanning.

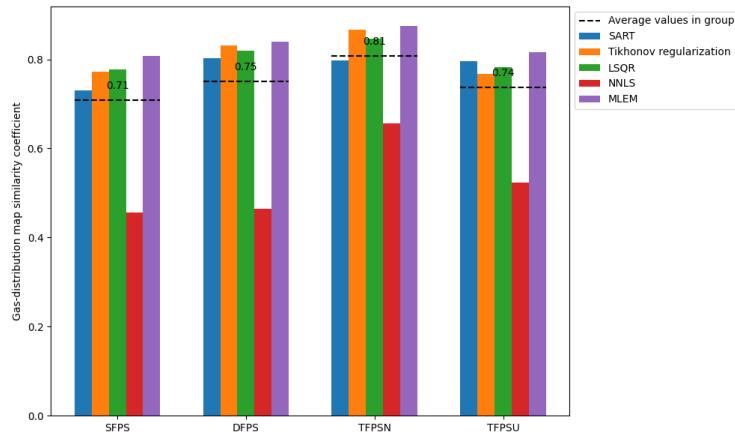


Figure 9. Gas-distribution map similarity coefficient of different algorithms under 16×16 grid cells and different type of configurations of laser scanning

It follows from Figure 9, among the algorithms the MLEM consistently achieves the highest similarity coefficient across all configurations. Furthermore, the TFPSN configuration yields the highest gas-distribution map similarity coefficient compared to the other scanning configurations, regardless of the algorithm used.

Conclusion

This paper presented a general review of gas distribution mapping using TDLAS, focusing on the impact of laser scanning configurations and tomographic reconstruction algorithms. The findings underscore the role of scanning configuration and algorithm selection in enhancing reconstruction accuracy.

Among the tomographic algorithms, MLEM consistently achieved the highest gas-distribution map similarity coefficient, demonstrating its robustness in handling complex and noisy datasets;

The TFPSN configuration provided the best reconstruction accuracy among the four tested configurations, achieving a superior balance between coverage and computational efficiency.

By understanding the behavior of light interactions with gas molecules and surfaces, and optimizing scanning parameters, this study offers significant advancements in the accuracy and efficiency of GDM systems.

References

1. Theophanides M., Anastassopoulou J. // *J. Environ. Sci. Health A Tox. Hazard. Subst. Environ. Eng.* 2009. Vol. 44. P. 758–766.
2. Wang X., Qian C., Zhao Z., Li J. and Jiao M. // *Chemosensors*. 2023. Vol. 11. P. 96–110.
3. Aoki T., Ohka S., Shiozawa D., Ogawa Y., Sakagami T. // *Engineering Proceedings*. 2023. Vol. 51, P. 44–55.
4. Hu Y., Xu L., Shen X., Jin L. // *Applied Optics*. 2021. Vol. 60. P. 9396–9403.
5. Log T., Pedersen W.B., Moumets H. // *Energies*. 2019. Vol. 12. P. 1454–1464.
6. Wang D., Li Y., Pu Y. // *Sensors*. 2024. Vol. 24. P. 1307–1321.
7. Sun Y., Chen W., Li F., Gu Z., Feng L., Guo D. and Cai H. // *IEEE Transactions on Instrumentation and Measurement*. 2023 Feb. Vol. 72. P.1–11.
8. Pradhan R. K. // *Science*. 2015. Vol. 28. P. 31–40.
9. Stewart Q. J. // *Opt. Soc. Am.* 1925. Vol. 11. P. 581–597.